Electrochimica Acta 427 (2022) 140873

Contents lists available at ScienceDirect

Electrochimica Acta

journal homepage: www.journals.elsevier.com/electrochimica-acta

Electrochemical characterization of alloy segregation in the near-surface deformed layer of welded zones of an Al−Cu−Li alloy using scanning electrochemical microscopy

Rejane Maria P. da Silva [a,*], Javier Izquierdo [b,c], Mariana X. Milagre [a], João Victor de S. Araujo [a], Renato A. Antunes [d], Ricardo M. Souto [b,c,*], Isolda Costa [a,*]

[a] Materials Science and Technology Center, Instituto de Pesquisas Energéticas e Nucleares, Nuclear and Energy Research Institute – IPEN/CNEN – Av. Prof. Lineu Prestes, São Paulo, SP 2242, Brazil
[b] Department of Chemistry, Universidad de La Laguna, P.O. Box 456, La Laguna (Tenerife), Canary Islands E-38200, Spain
[c] Institute of Material Science and Nanotechnology, Universidad de La Laguna, P.O. Box 456, La Laguna (Tenerife), Canary Islands E-38200, Spain
[d] Center for Engineering, Modeling and Applied Social Sciences (CECS), Federal University of the ABC (UFABC), Santo André, SP 09210-580, Brazil

ARTICLE INFO

Keywords:
2098-T351 Al alloy
Friction stir welding
Near-surface deformed layer
Localized electrochemical activity
SECM
Mg^{2+} ion-selective microelectrode

ABSTRACT

The development of heterogeneous electrochemical activity in the welded zones of aluminum alloy 2098-T351 by friction stir welding (FSW) associated with the formation of a near-surface deformed layer (NSDL) upon exposure to an aqueous chloride-containing solution was characterized using scanning electrochemical microscopy (SECM) in potentiometric operation. A solid-contact Mg^{2+} ion-selective microelectrode allowed in situ monitoring of the corrosion reactions sites for magnesium dissolution from different zones of the FSW weld upon exposure to a chloride-containing aqueous environment. In this way, localized corrosion reactions developing in the galvanically coupled joint/heat affected zones (WJ/HAZ) of the weld were detected and imaged with spatial resolution. The most active domains for local Mg^{2+} concentrations were associated with the HAZ of the retreating side (RS), and these corresponded to Mg oxidation from the Mg-enriched oxide bands in NSDL.

1. Introduction

During Al alloy manufacturing processes, such as machining, rolling, extrusion, and mechanical grinding, among others, high shear deformation causes severe plastic strain, forming a near-surface deformed layer (NSDL) in the material [1–4]. This deformation layer exhibits different characteristics from the bulk alloy, namely ultrafine grains and the segregation of alloying elements at the grain boundaries. This happens because in the NSDL, hardening precipitates, which may initially be contained in the material, may dissolve into the alloy matrix during machining. Subsequently, alloying elements, such as Mg and Zn, may segregate at the grain boundaries of the newly produced fine grains in the NSDL [2,5,6], exhibiting microstructures different from those of the bulk material [2,7–10]. In addition, the NSDL significantly influences the corrosion behavior of metallic alloys due to high dislocation densities and residual stresses [3,11–14]. As a result, the NSDL is more susceptible to corrosion than bulk material when exposed to an aerated aqueous solution containing chloride ions at ambient temperature and corrodes preferentially over the raw alloy [5,15]. A near-surface deformed layer is also formed during friction stir welding (FSW) [16], a solid-state process employed for Al alloys which leads to the development of different zones in addition to the unaffected base material, i.e. a thermomechanically affected zone (TMAZ) and a stir zone (SZ) constituting the welded joint (WJ), and a heat-affected zone (HAZ) [16–19]. The development of macrogalvanic corrosion processes due to the coupling between weld zones of different microstructure has been shown for the 2198-T851 alloy using the scanning vibrating electrode technique (SVET) and localized electrochemical impedance spectroscopy (LEIS) [20–23]. Although these microelectrochemical methods lacked chemical specificity, i.e. metal dissolution could not be unambiguously attributed to a specific element for a given anodic site, they did help identify sites of cathodic or anodic activity.

Chemically resolved information on local electrochemical activities developed in welded regions should be available using scanning electrochemical microscopy (SECM) with amperometric tips, but they were only able to provide indirect determinations related to oxygen

* Corresponding authors.
E-mail addresses: rejane.silva@ipen.br (R.M.P. da Silva), rsouto@ull.es (R.M. Souto), icosta@ipen.br (I. Costa).

https://doi.org/10.1016/j.electacta.2022.140873
Received 9 March 2022; Received in revised form 5 July 2022; Accepted 16 July 2022
Available online 17 July 2022

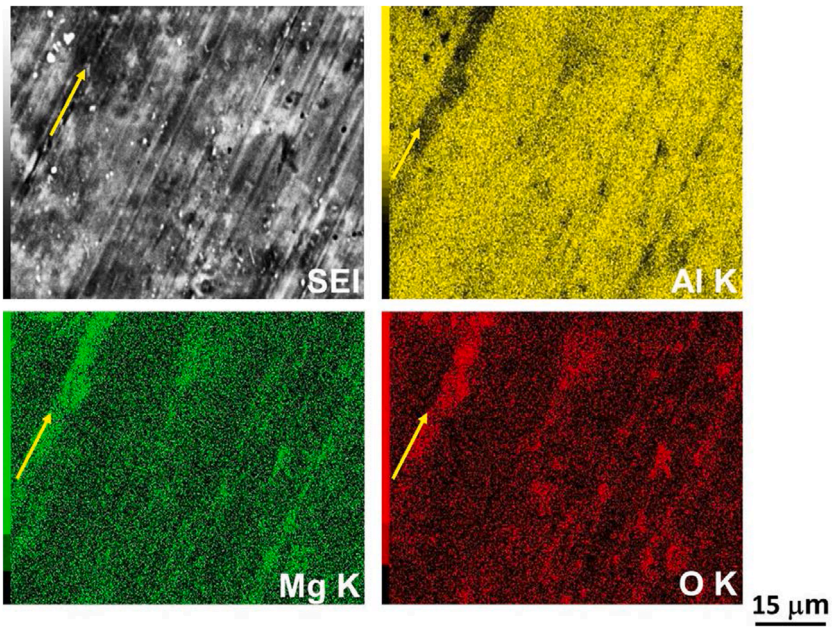

Fig. 1. SEM image and corresponding EDX distribution maps for Al, Mg and O of the as received 2098-T351 Al alloy.

consumption in the cathodic sites or local variations in surface reactivity [17,20,24]. The reason for this situation is the limited applicability of these probes for the characterization of highly reactive metals that release ionic species with very negative redox potentials (such as aluminum and magnesium) in aqueous environments [25–27]. More recently, a potentiometric probe in combination with a conventional amperometric SECM tip was used to study the electrochemical behavior of coupled FSW weld zones in 2098-T351 Al-Cu-Li [28], as well as its parent material, which has led to the observation that the anodic activity develops preferentially in the HAZ region of the weld. Unfortunately, these studies were performed using the alloy surfaces in a polished state, thus effectively after removal of the NSDL, and therefore did not address the effect of the developed Mg-enriched bands in the NSDL due to metal segregation [15]. Since Mg is a highly reactive metal, it should influence the corrosion activity of as-received alloys with an NSDL. Until now, the specific electrochemical characteristics derived from metal segregation in the alloy have not been obtained.

An alternative procedure to obtain the specific electrochemical activity of a certain metal in an alloy system would be to use an ion-selective microelectrode (ISME) as the tip for the SECM in potentiometric operation [29,30], a procedure already used to monitor metal dissolution from various model galvanic corrosion systems, including cases involving aluminum or magnesium [31–33]. Therefore, this work aims to provide more information on the interfacial and surface chemistry associated with the NSDL in the adjacent zones of the weld joint produced by FSW in the Al-Cu-Li alloy 2098-T351 when exposed to an aqueous NaCl solution using a solid contact Mg^{2+} ion-selective microelectrode (Mg^{2+}–ISME). Although Mg^{2+}–ISME has previously been used to monitor Mg^{2+} ion distributions from pure magnesium or a magnesium alloy exposed to aqueous electrolyte environments [31,32], no designed attempt has been made to detect the small amounts of the metal (~0.3 wt%) present as a minor alloying element in an alloy such as 2098-T351, nor to detect heterogeneous electrochemical activities resulting from the segregation of magnesium during the FSW process. To support the microelectrochemical observations, information on the surface composition in the different weld zones of the alloy was obtained by X-ray Photoelectron Spectroscopy (XPS).

2. Experimental

2.1. Material

The composition in wt% of the 2098-T351 Al-Cu-Li alloy is 3.4 Cu, 1.0 Li, 0.3 Mg, 0.3 Ag, 0.4 Zr, 0.04 Fe, 0.05 Si, 0.02 Zn, 0.003 Mn. The alloy was investigated in the welded condition without grinding or polishing (i.e., the sample material presented the corresponding NDSL). The FSW process was carried out at the Brazilian Nanotechnology National Laboratory (LNNano, Brazilian Center for Research in Energy and Materials, Campinas, SP, Brazil) employing a rotation rate of 1000 rpm and a transverse speed of 150 mm min^{-1}. The diameters of the tool shoulder and the pin were 10 mm and 5 mm, respectively. The surfaces were thoroughly rinsed with deionized water and ethanol before analysis.

2.2. Surface characterization

Scanning electron microscopy (SEM) coupled with Energy Dispersive X-ray Spectroscopy (EDX) using a JEOL JSM-6010LA microscope was employed to reveal the morphology and semi-quantitative composition of the surface of the as-received 2098-T351 Al-Cu-Li alloy in areas of interest, with an analysis depth of approximately 1 μm.

X-ray Photoelectron Spectroscopy (XPS) was used to obtain high resolution Mg2p and O1s spectra of the different weld zones of the alloy produced by the FSW process in order to determine the elemental composition and the possible presence of oxide layers in the first few nanometres of the surface. A Thermo Fisher Scientific K-Alpha+ spectrometer working with a monochromatic Al K-α X-ray source (1486.6 eV), (Waltham, MA, USA) was used. The spot size was 400 μm, the pass energy was 50 eV, and the pressure in the analysis chamber was around 10^{-7} Pa. The energy scale was calibrated against the adventitious C1s peak (284.8 eV). Prior to spectra acquisition, the sample surface was cleaned with isopropyl alcohol, followed by conventional cleaning with an argon ions stream at a medium current level for 60 s.

The surfaces of the as received alloy samples retrieved after immersion corrosion tests in a 5 mmol L^{-1} NaCl solution for periods of exposure to the test solution of up to 16 h at room temperature were characterized using an optical microscope (Leica DMLM; Wetzlar, Germany) coupled to a Leica EC3 camera, controlled by *LASES*® software.

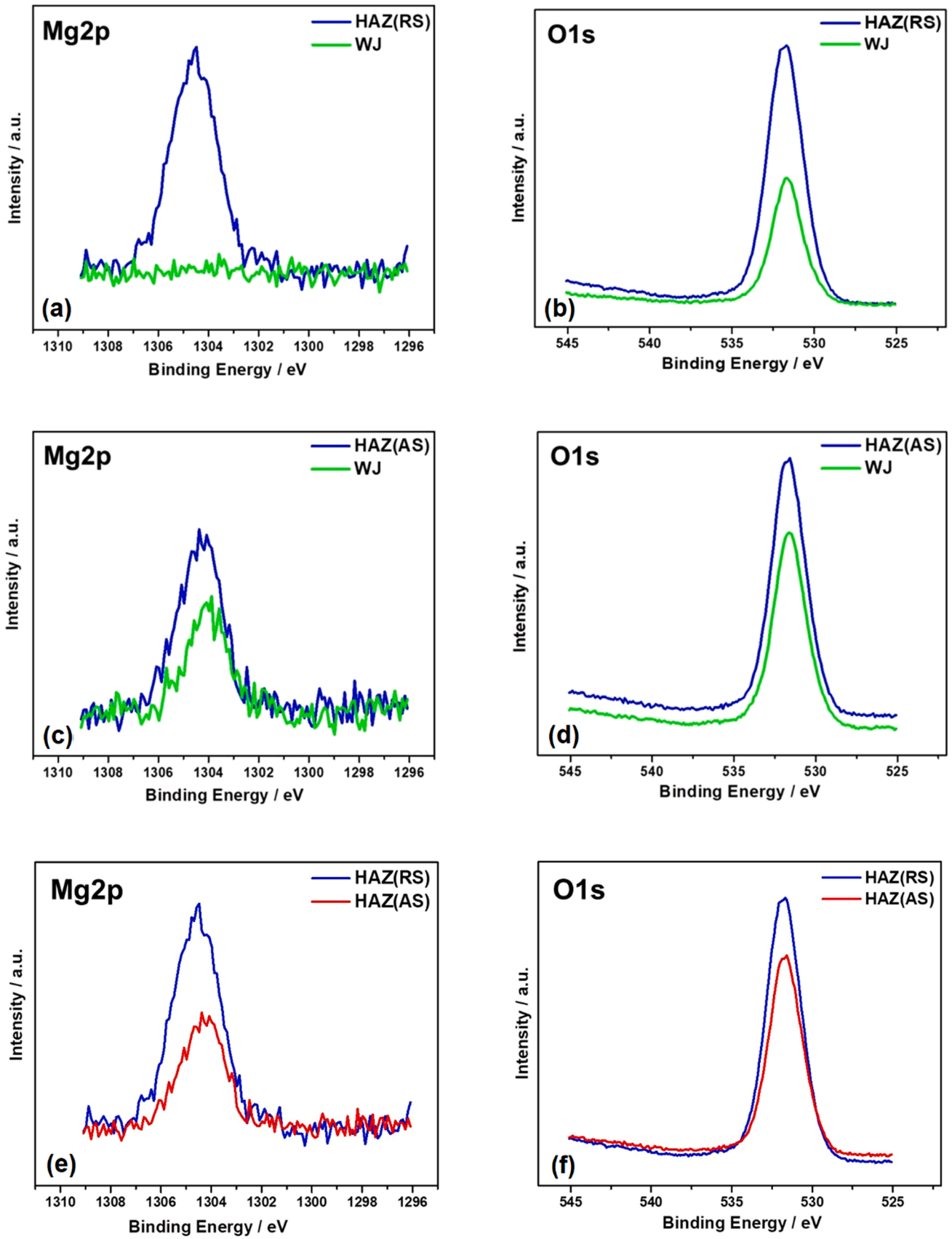

Fig. 2. High resolution Mg2p and O1s spectra measured by XPS in the welding zones of the as received FSW 2098-T351 Al alloy: (a and b) the WJ/HAZ in the retreating side (RS), (c and d) the WJ/HAZ in the advancing side (AS), and (e and f) the HAZ regions (in both RS and AS).

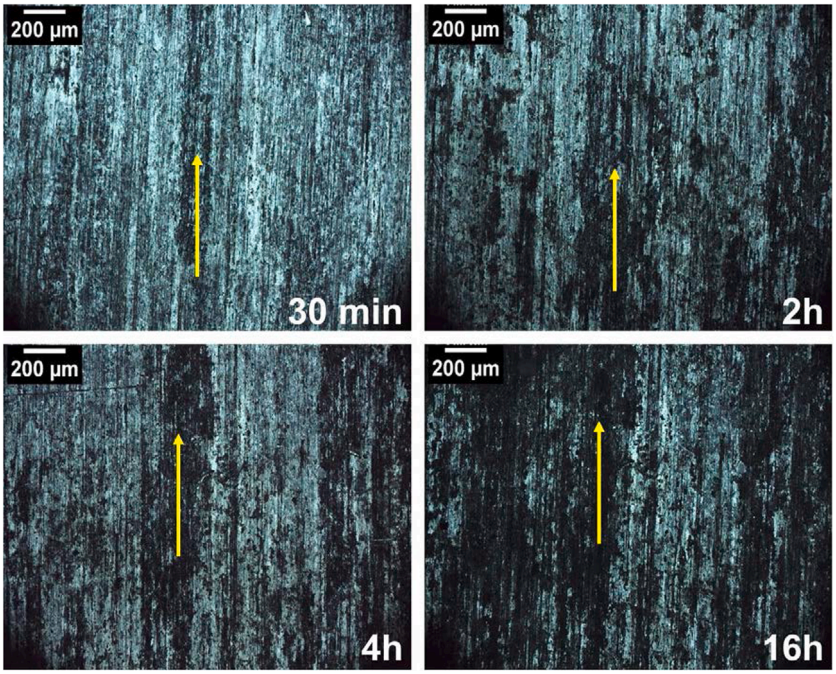

Fig. 3. Optical images of the as received 2098-T351 Al alloy after exposure in 5 mmol L^{-1} NaCl solution for different time periods as indicated. Arrows indicate the NSDL bands.

2.3. Scanning electrochemical microscopy

The microelectrochemical investigation was performed using a SECM apparatus (Sensolytics, Bochum, Germany), connected to an Autolab electrochemical interface (Metrohm, Herisau, Switzerland). To achieve the potentiometric operation, a 10^{12} Ω input impedance operational amplifier (TL071, Texas Instruments, Dallas, TX, USA) was introduced in the voltage follower clamp of the measuring circuit. The SECM probe was a solid contact Mg^{2+}–ISME, and the fabrication, response time determination, and calibration procedures for this ISME have been described elsewhere [31]. A Nerstian behavior with a slope −29.2 mV $decade^{-1}$ and response times between 0.2 – 0.3 s were determined.

The electrochemical cell included an Ag/AgCl/KCl (sat.) reference electrode in addition to the Mg^{2+}–ISME for the potentiometric operation, while the FSW 2098-T351 Al-Cu-Li alloy was placed at the bottom of the cell with its NSDL facing the electrolytic solution. The latter was left unpolarized in the cell. The ISME was positioned at a fixed height (~80 µm) above the surface; the vertical tip-substrate distance was established using the gentle approach procedure with the aid of a video camera television system. The SECM maps were recorded using a scan rate of 50 µm s^{-1} and *X-Y* increments: 25–50 µm, respectively.

3. Results and discussion

3.1. Surface characterization of the NSDL formed in the weld

The occurrence of Mg- and O-rich bands in the NSDL in the rolling direction for the as-received FSW-welded 2098-T351 Al alloy due to the FSW process is supported by the SEM micrograph and EDX maps shown in Fig. 1 (as indicated by the yellow arrows). It has been reported in the literature that Mg enrichment in the NSDL occurs due to outward diffusion of Mg during hot working steps [2,34], and this effect was related to the high temperatures reached in the fabrication process, which favored the migration of Mg to the surface and, consequently, its oxidation. The oxidation process would lead to the formation of MgO and the reduction of amorphous alumina, forming the oxide layer on the surface [35]. Analogously, alloy segregation and heterogeneous Mg-distribution in FSW-2098-T351 aluminum can be associated with the temperatures reached in the weld. Higher temperatures are reached in the AS (i.e. >400 °C) compared to the RS (<400 °C) [36] thus favoring the presence of the NSDL in the latter because the oxidation of Mg is favored at temperatures above 400 °C [39]. As the Mg oxidation rate increases, the Mg content tends to decrease. Next, Mg oxidation and diffusion rates at the surface increase with temperature [10,37]. Thus, due to the higher temperatures reached in the AS, the Mg content in this region decreases, as it tends to oxidize and, therefore, the Mg content in the formed oxide bands will be smaller.

Therefore, the different zones developed in the weld region were also characterized by XPS obtaining the high resolution Mg2p and O1s spectra of Fig. 2. Although O1s peaks were observed in the four regions considered (see Fig. 2b and d), Mg2p peaks were obtained in all cases but the WJ coupled with the HAZ(RS), in which no Mg2p signal was detected (see Fig. 2a and c). Furthermore, differences in Mg2p and O1s signals were detected in the HAZ (AS) compared to HAZ(RS) as shown in Fig. 2e and f, with higher signals recorded in the HAZ(RS). Therefore, it is in this region that the most Mg-enriched bands appear. Moreover, the Mg2p peaks around 1304 eV are generally attributed to Mg oxide [38, 39], and the presence of magnesium oxides in these regions was confirmed by inspecting the O1s spectra shown in Fig. 2c and d.

3.2. Spatially-resolved microelectrochemical investigation using the Mg^{2+}–ISME

Changes in the surface of the 2098-T351 alloy associated with a corrosive attack in a 5 mmol L^{-1} NaCl solution were first imaged using optical microscopy at different exposure times. In this way, corrosion propagation related to the Mg-enriched bands (indicated by the yellow arrows in Fig. 3) could be noted from a large accumulation of corrosion products in these regions. The corrosion activity in these bands started from the first minutes of immersion and gradually increased with time (cf. Fig. 3a).

Potentiometric SECM tests were performed using the Mg^{2+}–ISME to image spatially resolved pMg^{2+} distributions developing in the electrolyte adjacent to FSW 2098-T351 Al alloy during 2 h immersion in 5 mmol L^{-1} NaCl solution. The electrochemical activity that develops at

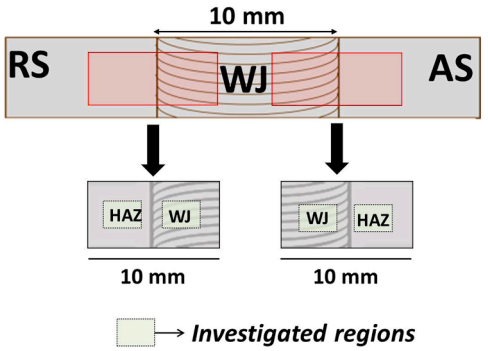

Fig. 4. Sketch of the as received FSW 2098-T351 showing the regions monitored during the microelectrochemical investigation.

each of the coupled WJ/HAZ interfaces formed in the alloy on both the receding side (RS) and on the advancing side (AS) of the welding were determined by exposing them separately to the test electrolyte as shown in Fig. 4.

Fig. 5 shows the local concentration distributions of Mg^{2+} ions as 2D array scan maps. They evidence a localized corrosion attack with more active domains for Mg^{2+}dissolution in the HAZ zones compared to the WJ zones, and this activity is more intense in the RS. A galvanic coupling mechanism can be associated to the welded zones of friction stir welded 2098-T351 aluminum alloy as received, considering that the Mg-rich bands were removed from the WJ zone during the welding process, and the HAZ is richer in Mg, preferentially on the retreating side. Then, the HAZ is expected to be anodic compared to WJ, while higher Mg dissolution should occur in the HAZ regions. Indeed, the 2D array scan map in Fig. 5a, which was obtained in the HAZ(RS) zone, shows the highest concentrations of Mg^{2+} among all the regions, a feature that is particularly notorious when the HAZ(RS) is compared to the HAZ(AS) (see Fig. 5c). Furthermore, the shape of the concentration distributions in Fig. 5a corresponds to a localized band-like corrosion attack, which must be related to the Mg-enriched bands occurring in this region. Thus, when the Mg^{2+}-ISME passes over the Mg-enriched oxide band (NSDL), it detects the Mg^{2+} ions generated by the preferential dissolution of this metal. Since Mg^{2+} formation occurs preferentially in the NSDL and is favored in the HAZ(RS) during welding, the potentiometric SECM map given in Fig. 5a showing the HAZ(RS) activity corresponds to the higher Mg content in the oxide bands, and results in the observation of increased electrochemical activity in this region, where the attack is deeper compared to the adjacent regions of the alloy [40]0. This result confirms that the underlying bulk material is protected from corrosion due to the cathodic activity sustaining the anodic dissolution of the Mg-enriched band (NSDL), which is more active and therefore dissolves preferentially. This observation was confirmed by the optical micrographs shown in Fig. 6 which were made on the samples recovered after performing the SECM measurements. The occurrence of a localized corrosive attack in the form of bands was observed in the HAZ(RS) region, that is to say in the zone of greatest dissolution of Mg according to SECM (cf. Fig. 5).

In summary, the initial stages of corrosion in FSW 2098-T351 alloy is a highly localized electrochemical process that occurs in the near-surface deformed layer as result of alloy segregation during the FSW process. That is, the heterogeneous distribution of Mg along the weld leads to the anodic activation of the heat affected zone of the retreating side (i.e. HAZ(RS)) through a microgalvanic coupling mechanism in the joint/heat affected zones (WJ/HAZ) of the weld where the bulk material

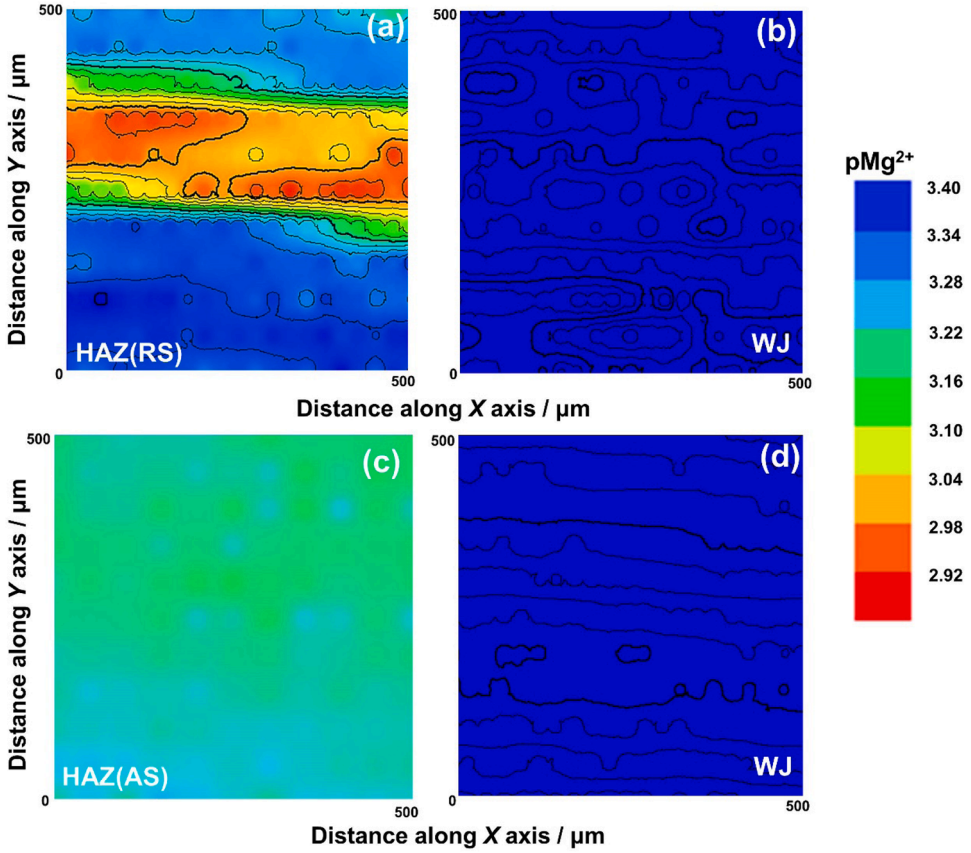

Fig. 5. Micropotentiometric mapping of local distributions of Mg^{2+} above coupled weldment zones (HAZ/WJ) of the (a and b) retreating side (RS) and (c and d) advancing side (AS) of the as received FSW 2098-T351 Al alloy while freely corroding in 5 mmol L^{-1} NaCl solution for about 2 h. The SECM maps were obtained using a Mg^{2+}-ISME for potentiometric SECM investigation. Tip-substrate distance: 80 µm; scan rate: 50 µm s^{-1}. ($pMg = -\log_{10}[Mg^{2+}]$).

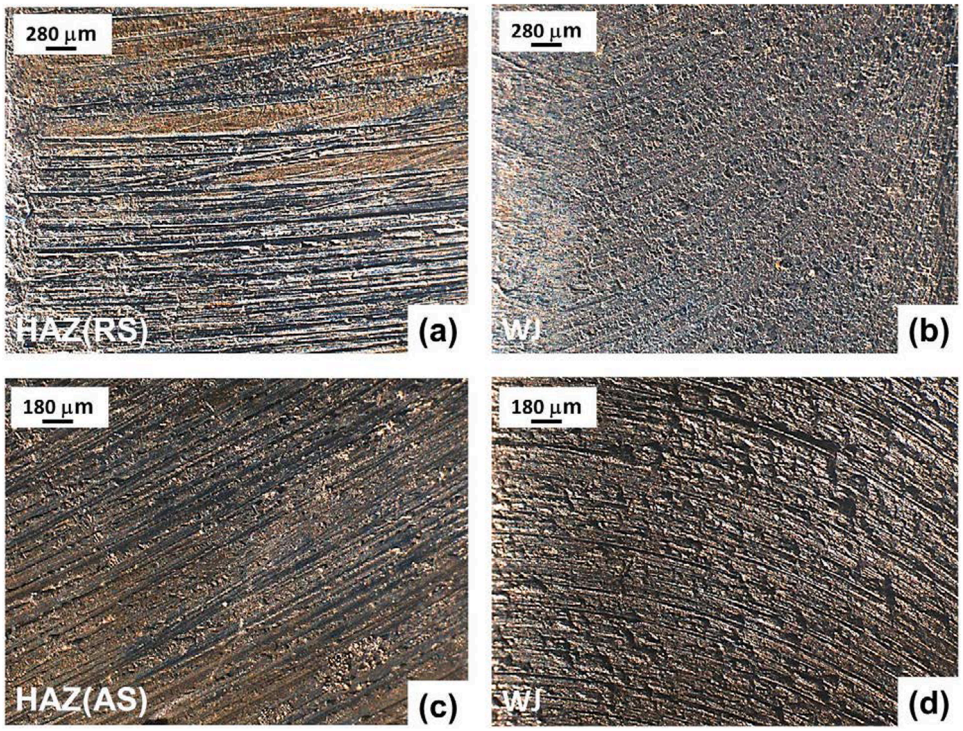

Fig. 6. Optical images of the coupled welded zones (HAZ/WJ) of the as received FSW 2098-T351 Al alloy retrieved after completion of SECM testing.

is protected against dissolution at this stage. This heterogeneous degradation process in the weld has been imaged in situ with chemical resolution for the first time using SECM in potentiometric mode, and has been largely ignored in the scientific literature due to the removal of the NSDL during surface preparation steps such as grinding and polishing, or chemical etching. In this way, the seemingly contradictory results observed in previous studies of this material which showed higher metal dissolution occurring on the advancing side than for RS from SVET maps [28] and when tracking the amount of Al^{3+} species that dissolve from the material [33] in polished samples of FSW 2098-T351. Such an apparent contradiction stems from the failure to detect the impact of magnesium dissolution from the anodic sites that develop in the HAZ (RS) after removal of NSDL during surface preparation.

4. Conclusions

The application of ISME potentiometric tips in SECM for the study of the local electrochemical behavior in the welding zones of Al alloys which present a near-surface deformed layer (NSDL) has been demonstrated in this work and can constitute a significant contribution in the field.The heterogeneous electrochemical activity across the weld produced on 2098-T351 aluminum alloy by friction stir welding upon exposure to an aqueous electrolyte solution was imaged in situ using a solid-contact Mg^{2+} ion-selective microelectrode as probe in the potentiometric operation of the SECM. In this way, a microgalvanic mechanism was observed to account for the localized corrosion process associated with the NSDL formed during the welding process.

The electrochemical activities in the coupled WJ/HAZ zones were studied separately. The potentiometric SECM results showed that the NSDL has an anodic electrochemical behavior with respect to the underlying bulk material. Localized corrosion attack occurred in the form of bands like the Mg-enriched bands that form during the FSW process, and the most active domains for Mg^{2+} dissolution were found in the HAZ (RS) region and exhibited band-like shapes.

High-resolution XPS spectra of the Mg2p and O1s signals obtained from the coupled WJ/HAZ zones, on both RS and AS sides, evidenced that Mg-enriched bands were preferentially found in the HAZ(RS), which was the region of highest electrochemical activity according to SECM measurements. Further observations of preferential corrosive attack in the HAZ(RS) were made by taking optical micrographs of the weld after completing the microelectrochemical and exposure tests in 5 mmol L^{-1} NaCl solution.

CRediT authorship contribution statement

Rejane Maria P. da Silva: Conceptualization, Investigation, Data curation, Validation, Visualization, Writing – original draft, Writing – review & editing. **Javier Izquierdo:** Data curation, Supervision, Visualization, Methodology, Writing – review & editing. **Mariana X. Milagre:** Investigation, Writing – review & editing. **João Victor de S. Araujo:** Investigation, Writing – review & editing. **Renato A. Antunes:** Investigation, Writing – review & editing. **Ricardo M. Souto:** Data curation, Supervision, Methodology, Funding acquisition, Writing – original draft, Writing – review & editing. **Isolda Costa:** Supervision, Resources, Funding acquisition, Writing – review & editing.

Declaration of Competing Interest

The authors declare that they have no known competing financial interests or personal relationships that could have appeared to influence the work reported in this paper.

Acknowledgements

The authors acknowledge Fundação de Amparo à Pesquisa do Estado de São Paulo (FAPESP; Proc. 2013/13235-6, Proc.2018/06880-6 and Proc. 2019/11427-1), as well as the University of La Laguna and the Spanish Ministry of Science, Innovation and Universities (Madrid, Spain) under contract No. 2022/0000586, for financial support. The Multiuser Central Facilities (CEM) of UFABC is acknowledged for the experimental support.

References

[1] G.M. Scamans, M.F. Frolish, W.M. Rainforth, Z. Zhou, Y. Liu, X. Zhou, G. E. Thompson, The ubiquitous Beilby layer on aluminium surfaces, Surf. Interface Anal. 42 (2010) 175–179, https://doi.org/10.1002/sia.3204.

[2] X. Zhou, Y. Liu, G.E. Thompson, G.M. Scamans, P. Skeldon, J.A. Hunter, Near-surface deformed layers on rolled aluminum alloys, Metall. Mater. Trans. A 42 (2011) 1373–1385, https://doi.org/10.1007/s11661-010-0538-2.

[3] Y. Liu, T. Hashimoto, X. Zhou, G.E. Thompson, G.M. Scamans, W.M. Rainforth, J. A. Hunter, Influence of near-surface deformed layers on filiform corrosion of AA3104 aluminium alloy, Surf. Interface Anal. 45 (2013) 1553–1557, https://doi.org/10.1002/sia.5232.

[4] J. Wang, X. Zhou, G.E. Thompson, J.A. Hunter, Y. Yuan, Microstructure evolution in the near-surface region during homogenization of a twin-roll cast AlFeMnSi alloy, Metall. Mater. Trans. A 47 (2016) 4268–4275, https://doi.org/10.1007/s11661-016-3568-6.

[5] B. Liu, X. Zhang, X. Zhou, T. Hashimoto, J. Wang, The corrosion behaviour of machined AA7150-T651 aluminium alloy, Corros. Sci. 126 (2017) 265–271, https://doi.org/10.1016/j.corsci.2017.07.008.

[6] B. Liu, X. Zhou, T. Hashimoto, X. Zhang, J. Wang, Machining introduced microstructure modification in aluminium alloys, J. Alloys Compd. 757 (2018) 233–238, https://doi.org/10.1016/j.jallcom.2018.05.082.

[7] M.F. Frolish, J.C. Walker, C. Jiao, W.M. Rainforth, J.H. Beynon, Formation and structure of a subsurface layer in hot rolled aluminium alloy AA3104 transfer bar, Tribol. Int. 38 (2005) 1050–1058, https://doi.org/10.1016/j.triboint.2005.07.021.

[8] Y. Liu, M.F. Frolish, W.M. Rainforth, X. Zhou, G.E. Thompson, G.M. Scamans, J. A. Hunter, Evolution of near-surface deformed layers during hot rolling of AA3104 aluminium alloy, Surf. Interface Anal. 42 (2010) 180–184, https://doi.org/10.1002/sia.3135.

[9] J. Wang, X. Zhou, G.E. Thompson, J.A. Hunter, Y. Yuan, Delamination of near-surface layer on cold rolled AlFeSi alloy during sheet forming, Mater. Charact. 99 (2015) 109–117, https://doi.org/10.1016/j.matchar.2014.11.011.

[10] J. Wang, X. Zhou, G.E. Thompson, J.A. Hunter, Y. Yuan, Near-surface microstructure on twin-roll cast 8906 aluminum alloy, Metall. Mater. Trans. A 46 (2015) 2688–2695, https://doi.org/10.1007/s11661-015-2877-5.

[11] A. Afseth, J.H. Nordlien, G.M. Scamans, K. Nisancioglu, Effect of thermo-mechanical processing on filiform corrosion of aluminium alloy AA3005, Corros. Sci. 44 (2002) 2491–2506, https://doi.org/10.1016/S0010-938X(02)00036-7.

[12] X. Zhou, G.E. Thompson, G.M. Scamans, The influence of surface treatment on filiform corrosion resistance of painted aluminium alloy sheet, Corros. Sci. 45 (2003) 1767–1777, https://doi.org/10.1016/S0010-938X(03)00003-9.

[13] Y. Liu, A. Laurino, T. Hashimoto, X. Zhou, P. Skeldon, G.E. Thompson, G. M. Scamans, C. Blanc, W.M. Rainforth, M.F. Frolish, Corrosion behaviour of mechanically polished AA7075-T6 aluminium alloy, Surf. Interface Anal. 42 (2010) 185–188, https://doi.org/10.1002/sia.3136.

[14] J. Seong, F. Yang, F. Scheltens, G.S. Frankel, N. Sridhar, Influence of the altered surface layer on the corrosion of AA5083, J. Electrochem. Soc. 162 (2015) C209–C218, https://doi.org/10.1149/2.0321506jes.

[15] U. Donatus, J.V.S. Araujo, C.S.C. Machado, N.V.V. Mogili, R.A. Antunes, I. Costa, The effect of manufacturing process induced near-surface deformed layer on the corrosion behaviour of AA2198-T851 Al–Cu–Li alloy, Corros. Eng. Sci. Technol. 54 (2019) 205–215, https://doi.org/10.1080/1478422X.2018.1558932.

[16] P.L. Threadgill, A.J. Leonard, H.R. Shercliff, P.J. Withers, Friction stir welding of aluminium alloys, Int. Mater. Rev. 54 (2009) 49–93, https://doi.org/10.1179/174328009X411136.

[17] U. Donatus, R.M.P. da Silva, J.V.S. Araujo, M.X. Milagre, C.P. de Abreu, C.S. C. Machado, I. Costa, Macro and microgalvanic interactions in friction stir weldment of AA2198-T851 alloy, J. Mater. Res. Technol. 8 (2019) 6209–6222, https://doi.org/10.1016/j.jmrt.2019.10.015.

[18] R.W. Fonda, J.F. Bingert, Precipitation and grain refinement in a 2195 Al friction stir weld, Metall. Mater. Trans. A 37 (2006) 3593–3604, https://doi.org/10.1007/s11661-006-1054-2.

[19] R. Nandan, T. Debroy, H.K.D.H. Bhadeshia, Recent advances in friction stir welding – process, weldment structure and properties, Prog. Mater. Sci. 53 (2008) 980–1023, https://doi.org/10.1016/j.pmatsci.2008.05.001.

[20] D. Sidane, E. Bousquet, O. Devos, M. Puiggali, M. Touzet, V. Vivier, A. Poulon-Quintin, Local electrochemical study of friction stir welded aluminum alloy assembly, J. Electroanal. Chem. 737 (2015) 206–211, https://doi.org/10.1016/j.jelechem.2014.06.025.

[21] J.C.B. Bertoncello, S.M. Manhabosco, L.F.P. Dick, Corrosion study of the friction stir lap joint of AA7050-T76511 on AA2024-T3 using the scanning vibrating electrode technique, Corros. Sci. 94 (2015) 359–367, https://doi.org/10.1016/j.corsci.2015.02.029.

[22] C.P. de Abreu, I. Costa, H.G. de Melo, P. Nadine, B. Tribollet, V. Vivier, Multiscale electrochemical study of welded Al alloys joined by friction stir welding, J. Electrochem. Soc. 164 (2017) C735–C746, https://doi.org/10.1149/2.0391713jes.

[23] F.M. Queiroz, U. Donatus, O.M.P. Ramirez, J.V.S. Araujo, B.V.G. de Viveiros, S. Lamaka, M. Zheludkevich, M. Masoumi, V. Vivier, I. Costa, H.G. de Melo, Effect of unequal levels of deformation and fragmentation on the electrochemical response of friction stir welded AA2024-T3 alloy, Electrochim. Acta 313 (2019) 271–281, https://doi.org/10.1016/j.electacta.2019.04.137.

[24] M.X. Milagre, U. Donatus, N.V. Mogili, R.M.P. Silva, B.V.G. de Viveiros, V. F. Pereira, R.A. Antunes, C.S.C. Machado, J.V.S. Araujo, I. Costa, Galvanic and asymmetry effects on the local electrochemical behavior of the 2098-T351 alloy welded by friction stir welding, J. Mater. Sci. Technol. 45 (2020) 162–175, https://doi.org/10.1016/j.jmst.2019.11.016.

[25] A.M. Simões, D. Battocchi, D.E. Tallman, G.P. Bierwagen, SVET and SECM imaging of cathodic protection of aluminium by a Mg-rich coating, Corros. Sci. 49 (2007) 3838–3849, https://doi.org/10.1016/j.corsci.2007.03.045.

[26] S.S. Jamali, S.E. Moulton, D.E. Tallman, M. Forsyth, J. Weber, G.G. Wallace, Applications of scanning electrochemical microscopy (SECM) for local characterization of AZ31 surface during corrosion in a buffered media, Corros. Sci. 86 (2014) 93–100, https://doi.org/10.1016/j.corsci.2014.04.035.

[27] S. Thomas, J. Izquierdo, N. Birbilis, R.M. Souto, Possibilities and limitations of scanning electrochemical microscopy of Mg and Mg alloys, Corrosion 71 (2015) 171–183, https://doi.org/10.5006/1483.

[28] R.M.P. da Silva, J. Izquierdo, M.X. Milagre, A.M. Betancor-Abreu, L.A. de Oliveira, R.A. Antunes, R.M. Souto, I. Costa, On the local corrosion behavior of coupled welded zones of the 2098-T351 Al-Cu-Li alloy produced by friction stir welding (FSW): an amperometric and potentiometric microelectrochemical investigation, Electrochim. Acta 373 (2021), 137910, https://doi.org/10.1016/j.electacta.2021.137910.

[29] B.R. Horrocks, M.V. Mirkin, D.T. Pierce, A.J. Bard, G. Nagy, K. Toth, Scanning electrochemical microscopy. 19. Ion-selective potentiometric microscopy, Anal. Chem. 65 (1993) 1213–1224, https://doi.org/10.1021/ac00057a019.

[30] G. Nagy, L. Nagy, Electrochemical sensors developed for gathering microscale chemical information, Anal. Lett. 40 (2007) 3–38, https://doi.org/10.1080/00032710600867226.

[31] J. Izquierdo, A. Kiss, J.J. Santana, L. Nagy, I. Bitter, H.S. Isaacs, G. Nagy, R. M. Souto, Development of Mg^{2+} ion-selective microelectrodes for potentiometric scanning electrochemical microscopy monitoring of galvanic corrosion processes, J. Electrochem. Soc. 160 (2013) C451–C459, https://doi.org/10.1149/2.001310jes.

[32] S.H. Salleh, N. Birbilis, M. Musameh, K. Venkatesan, S. Thomas, On the development and application of an in-house fabricated Mg^{2+} ion selective microelectrode (ISME) for assessing Mg corrosion, J. Electrochem. Soc. 165 (2018) C771–C776, https://doi.org/10.1149/2.0591811jes.

[33] R.M.P. da Silva, J. Izquierdo, M.X. Milagre, R.A. Antunes, R.M. Souto, I. Costa, Development of an Al^{3+} ion-selective microelectrode for the potentiometric microelectrochemical monitoring of corrosion sites on 2098-T351 aluminum alloy surfaces, Electrochim. Acta 415 (2022), 140260, https://doi.org/10.1016/j.electacta.2022.140260.

[34] K. Shimizu, G.M. Brown, K. Kobayashi, P. Skeldon, G.E. Thompson, G.C. Wood, The early stages of high temperature oxidation of an Al-0.5 wt% Mg alloy, Corros. Sci. 40 (1998) 557–575, https://doi.org/10.1016/S0010-938X(97)00153-4.

[35] K. Li, X.R. Zhou, G.E. Thompson, J.A. Hunter, Y.D. Yuan, Evolution of near-surface deformed layers on AA3104 aluminium alloy, Mater. Sci. Forum. 765 (2013) 358–362, https://doi.org/10.4028/www.scientific.net/MSF.765.358.

[36] M.X. Milagre, N.V. Mogili, U. Donatus, R.A.R. Giorjão, M. Terada, J.V.S. Araujo, C. S.C. Machado, I. Costa, On the microstructure characterization of the AA2098-T351 alloy welded by FSW, Mater. Charact. 140 (2018) 233–246, https://doi.org/10.1016/j.matchar.2018.04.015.

[37] Q. Tan, A. Atrens, N. Mo, M.-.X. Zhang, Oxidation of magnesium alloys at elevated temperatures in air: a review, Corros. Sci. 112 (2016) 734–759, https://doi.org/10.1016/j.corsci.2016.06.018.

[38] N.C. Haider, J. Alonso, W.E. Swartz, Valence and core electron spectra of Mg in MgO in evoporated thin films, Z. Naturforsch. A 30 (1975) 1485–1490, https://doi.org/10.1515/zna-1975-1119.

[39] J.E. Qu, M. Ascencio, L.M. Jiang, S. Omanovic, L.X. Yang, Improvement in corrosion resistance of WE43 magnesium alloy by the electrophoretic formation of a ZnO surface coating, J. Coat. Technol. Res. 16 (2019) 1559–1570, https://doi.org/10.1007/s11998-019-00212-7.

[40] W.G. Barboza, M.X. Milagre, U. Donatus, C.S.C. Machado, O.M.P. Ramirez, J.V. S. Araujo, R.M.P. da Silva, I. Costa, Corrosion behaviour of the 2098-T351 Al–Cu–Li alloy after different surface treatments, Corros. Eng. Sci. Technol. 57 (2022) 1–11, https://doi.org/10.1080/1478422X.2022.2054915.